e-Journal of Nondestructive Testing - ISSN 1435-4934 - www.ndt.net

EWSHM 2024
11th European Workshop on Structural Health Monitoring

NDT Data-Supported Structural Reassessments based on Regression Relations in Measuring Data Analysis

Ardalan BAHRAMI ESKANDARI [1], Stefan KUETTENBAUM [1]
[1]Bundesanstalt für Materialforschung und -prüfung (BAM), division 8.2, Berlin, Germany.
Ardalan.bahrami-eskandari@bam.de
Stefan.Kuettenbaum@bam.de

Abstract. Non-destructive Testing (NDT) provides valuable data about structural elements, supporting the assessment of existing infrastructures without incurring additional structural damage from inspections. Simultaneously, the uncertainty in measurement, which quantifies the quality of measurement results, plays a crucial role in decisions aimed at, e.g., optimizing maintenance strategies, rehabilitation works and Structural Health Monitoring (SHM) implementations. The Guide to the Expression of Uncertainty in Measurement (GUM) framework has already been considered for non-destructive concrete testing. Regarding that, extensive measurements with sophisticated scopes need to be conducted by experts as an obligatory process.

This study illustrates how NDT results describing the inner structure of a concrete element can effectively support the reassessment of bridges in operation. To achieve this, the study considers the various measurable positions of the resisting longitudinal tendons of a bridge structure to investigate the displacement change under dynamic service loads.

Furthermore, this study aims to simplify and optimize existing NDT data analysis procedures by employing regression analysis, enabling the detection of structural features. This regression analysis yields a modifier for determining the correct depth of an object within the structural element. The method is validated through laboratory experiments, including the use of an ultrasonic measurement system. As a result, it provides unbiased and accurately measured results, while ensuring that the measurement data can remain uncorrelated. Major advantages include efficient computation, a wider scope, and avoiding redundant information about the measuring process.

The findings demonstrate that employing the proposed NDT analysis method, with its enhanced practicability, can significantly augment the efficiency of NDT data-supported structural reassessments across various scenarios.

Keywords: Existing structures, Non-destructive testing, Bridge reassessment, Statistical analysis, Practicality measurement.

https://doi.org/10.58286/29714

Introduction

The study of critical transportation infrastructure, namely bridge, has captured researchers' attention, particularly in the last two decades [1,2,3,4,5]. Various theoretical approaches, such as the Moving Mass/Load/Oscillator theories, have been employed to investigate dynamic loading on bridge structures when subjected to moving vehicles [6,7]. Moreover, researchers have explored methods to compute deflections, shape functions, and natural frequencies of bridges [8,9]. The combination of earthquake phenomena and moving vehicles has also been analysed to understand bridge deformations [10]. Additionally, bridge reliability assessment has been studied using methods like the First and Second Order Reliability Method (FORM and SORM), among others [11,12,13]. Assessing bridges directly depends on their structural characteristics, such as bridge type, material properties, section properties, flexural rigidity, and slenderness. Creating accurate models of bridges through various approaches like beam theories (EBT, TBT, HOBT) [1,8,9,10] or finite element methods (FEM) [11,12] is crucial for studying and understanding bridge structures.

However, more realistic modelling of existing structures can be achieved by knowing the specific positioning of resistance elements within the structural elements. The measurement process plays a pivotal role in constructing appropriate models, especially in cases with construction uncertainties or unknown historical structures. Non-destructive testing methods present a significant advantage in this regard, and they do also minimize additional damage or disruption caused by bridge inspections [12]. The evaluation and reassessment of existing bridge structures based on NDT data have been demonstrated [12], and the importance of considering uncertainty in the measurement process is emphasized [14].

This study focuses on evaluating bridge performance by considering different tendon positions within main beams. Numerical modeling employs Euler-Bernoulli beam theory and the Eigenfunction Expansion Method (EEM) to analyze maximum deflection at mid-span, a key indicator for Displacement Based Control (DBC). Investigation of an existing bridge structure shows that there is a performance variation for different tendon duct positions along the beam length during operational phases under the effect of traveling vehicles. Additionally, regression analysis is utilized to simplify NDT data analysis procedures, enabling the detection of structural features. This approach introduces a practical Ultrasonic NDT method for on-site measurements by engineers, providing a quick assessment of resistance element positioning within structural elements. A statistical study results in a regression function dependent on the position of the measuring device (PMD) within the structural elements, forming an integral component of a general mathematical constant velocity relation.

1. Displacement Based Control (DBC)

1.1 Formulation

Consider a simply supported bridge which is a uniform undamped single-span Euler-Bernoulli beam. It has a length of L, flexural rigidity $EI(x)$, and mass per unit length ρA. As shown in the following equation, $D(x,t)$ describes the function of vertical displacement along the beam length at time t [10].

$$\rho A \frac{\partial^2 D(x,t)}{\partial t^2} + EI(x) \frac{\partial^4 D(x,t)}{\partial x^4} = f(x,t) \quad (1)$$

The dynamic excitation occurs during its operation: a group of traveling vehicles, each with a constant velocity v and a mass of m_k, crosses the beam at uniformly determined

intervals of d. This dynamic situation is illustrated in Figure 1.

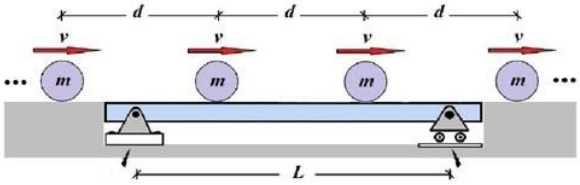

Fig. 1. Schematic view of situation [10].

To model the external dynamic loading, we employ the moving masses theory, expressed as:

$$f(x,t) = \sum_{k=1}^{N} m_k \left[g - \frac{d^2 D_0(t)}{dt^2} \right] . (\delta [x - v(t - t_k)] . \Delta H(t)) \quad (2)$$

Here, N represents the total number of vehicles, and $D_0(t)$ signifies the vertical displacement of the moving masses. The vehicles remain in contact with the beam throughout vibration, meaning $D_0(t) = D(x = v(t - t_k), t)$, where t_k denotes the time of arrival of the kth vehicle. $\Delta H(t) = H(t - t_k) - H\left(t - t_k - \frac{L}{v}\right)$ acts as a unit step function to describe the action of the kth mass as it enters and departs from the beam, respectively, and δ represents the Dirac delta function. By applying the Eigenfunction Expansion Method (EEM), where $D(x,t) = \sum_{i=1}^{p} \varphi_i(x) a_i(t)$, and considering Equation (1), we derive the matrix equation below. This involves multiplying both sides by $\varphi_j(x)$, integrating over the beam length (L), applying the orthogonal perpendicular principle, and calculating the orthogonal shape functions $\varphi_i(x)$ through characteristic orthogonal polynomials (COPs) [8] or using the direct method for simply supported beams [10]:

$$\boldsymbol{M}(\boldsymbol{t}) \frac{d^2 a(t)}{dt^2} + \boldsymbol{C}(\boldsymbol{t}) \frac{da(t)}{dt} + \boldsymbol{K}(\boldsymbol{t}) \boldsymbol{a}(\boldsymbol{t}) = \boldsymbol{F}(\boldsymbol{t}) \quad (3)$$

Where:

$$\begin{aligned}
&\boldsymbol{a}(\boldsymbol{t}) = [\boldsymbol{a_i}(\boldsymbol{t})]_{\boldsymbol{p\times 1}} \\
&\boldsymbol{M}(\boldsymbol{t}) = \left[\boldsymbol{\rho A \delta_{ij}} + \sum_{k=1}^{N} m_k \phi_i[v(t - t_k)] . \phi_j[v(t - t_k)] . \Delta H(t)\right]_{p\times p} \\
&\boldsymbol{C}(\boldsymbol{t}) = \left[\sum_{k=1}^{N} 2 m_k v \phi_{i,x}[v(t - t_k)] . \phi_j[v(t - t_k)] . \Delta H(t)\right]_{p\times p} \\
&\boldsymbol{K}(\boldsymbol{t}) = \left[\sum_{i=1}^{p} \left\{\sum_{j=1}^{p} \int_0^L EI(x) . \phi_{i,xxxx} \phi_j(x) dx\right\} + \sum_{k=1}^{N} m_k v^2 \phi_{i,xx}[v(t - t_k)] . \phi_j[v(t - t_k)] . \Delta H(t)\right]_{p\times p} \\
&\boldsymbol{F}(\boldsymbol{t}) = \left[[g] \sum_{k=1}^{N} m_k \phi_j[v(t - t_k)] . \Delta H(t)\right]_{p\times 1}
\end{aligned} \quad (4)$$

Various numerical methods can be employed to solve the above equation in the time domain.

1.2 Actual Bridge Structure

To analyse the vibration and the maximum deflection of the bridge structure under various positioning of resistance elements, we investigate an existing bridge structure known as the "Amperbruecke," located in Munich, Germany with the total length of $L = 38.45\, m$ and $\rho A = 12095\, kg/m$. Figure 2 a. shows the bridge, and Figure 2 b. provides the number of longitudinal tendon ducts and their center of gravity within the main beam length, along with section properties at the mid-span based on as-built data. The flexural rigidity ($EI(x)$) of the entire beam is a function of beam length. The center of gravity of tendons at each section changes due to the positions and the mount of the longitudinal tendons along the beam length. Figure 3.a illustrates changes in moment of inertia along the bridge length for different

positions of longitudinal tendons. The centers of gravity of tendons at mid-span (Y_{cgt}) could vary in the range between 8.2 cm and 26.06 cm based on section dimension capacity.

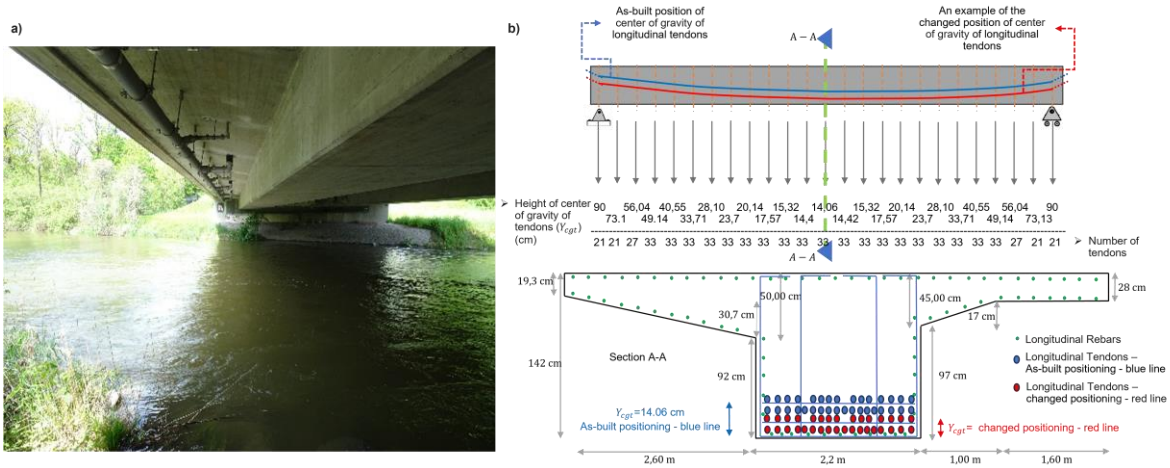

Fig. 2. a: "Amperbrücke" bridge structure, b: Positions of longitudinal tendons.

The change of Y_{cgt} at the middle cross section will be applied to the other cross sections along the entire beam length (refer to the red line in Fig2. b.). Moment of inertia is calculated using the equivalent section principle at each section, taking into account the absence of a crack zone due to the prestressed bridge type. As shown in Fig. 3a, the moment of inertia of the entire beam increases by decreasing Y_{cgt} and vice versa.

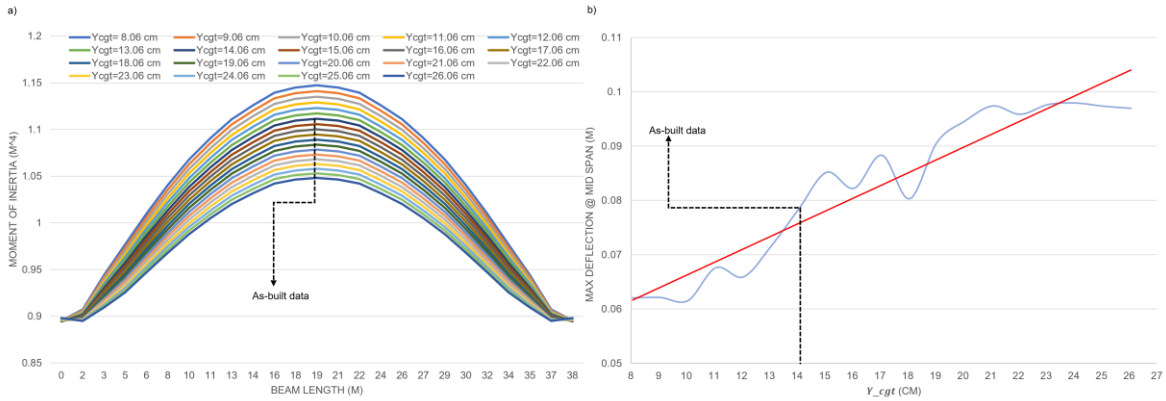

Fig. 3. The effect of different center of gravity of longitudinal tendon ducts in the bridge, a: variation of moment of inertia along the bridge length, b: change in maximum deflection at mid-span.

Figure 3.b depicts the maximum deflection at the mid-span of the bridge for various positions of the center of gravity of tendon ducts (blue line), along with the corresponding linear trend line variations (red line). These results are derived from the solution of equation (3) under the influence of a group of 15 traveling vehicles, each with a constant velocity $v = 30\,m/s$ and a mass of $m_k = 50000\,kg$, crossing the bridge at uniformly determined intervals of $d = L/2$ over a total time of 16 seconds [10]. The responses indicate a noticeable increase in the maximum deflection at mid-span as the center of gravity of the longitudinal tendon ducts (Y_{cgt}) increases. The variation in the position of the tendon duct causes approximately ±25% response difference compared to the as-built data. These findings underscore the significant impact of the placement of resistance elements in the bridge on the performance of beam-type structures. Such consequence should be considered in Structural Health Monitoring (SHM) processes or reassessing existing structures, which has deviations from the original construction plans or historical data.

In addition, Non-Destructive Testing (NDT) methods play a crucial role in extracting the actual structural properties of infrastructures without causing extra damage. To ensure the reliability of NDT results, it is essential having experts knowing signal processing and measurement techniques to compute and minimize measurement uncertainties. However, despite the necessity of investing sufficient time in these processes, practical constraints such as the presence of non-structural elements, architectural limitations, or the interference of mechanical facilities often impede optimal measurement processing. In the subsequent discussion, we focus on the development of rapid and practical NDT methods that are more efficient for addressing measurement uncertainties. This approach aims to enable all engineers to conduct NDT assessments effectively and covering the practical constraints, even without expertise in the field, by providing step-by-step guidance.

2. NDT Measuring Data Analysis

2.1 Measurement Process

Consider a measurement process using an ultrasonic measurement device with the objective of determining the depth (h_T) of a resistance object within a structural element, as illustrated in Figure 4. The position of the measurement device (PMD) is determined by coordinates X and Y, with an assumed origin at the corner and the center of the measurement device (C_d). The distance between the center of transducers (C_t) and C_d, as well as the distance between the center of receivers (C_r) and C_d, is denoted as S. The PMD's orientation can be described by the angles Θ and φ, which represent the PMD's orientation relative to the target of interest. Additionally, the boundary conditions in the specimen, with a length of A and width of B, are indicated by the angles α and β. The values of D and E are the lengths respective to the x and y axes within the specimen.

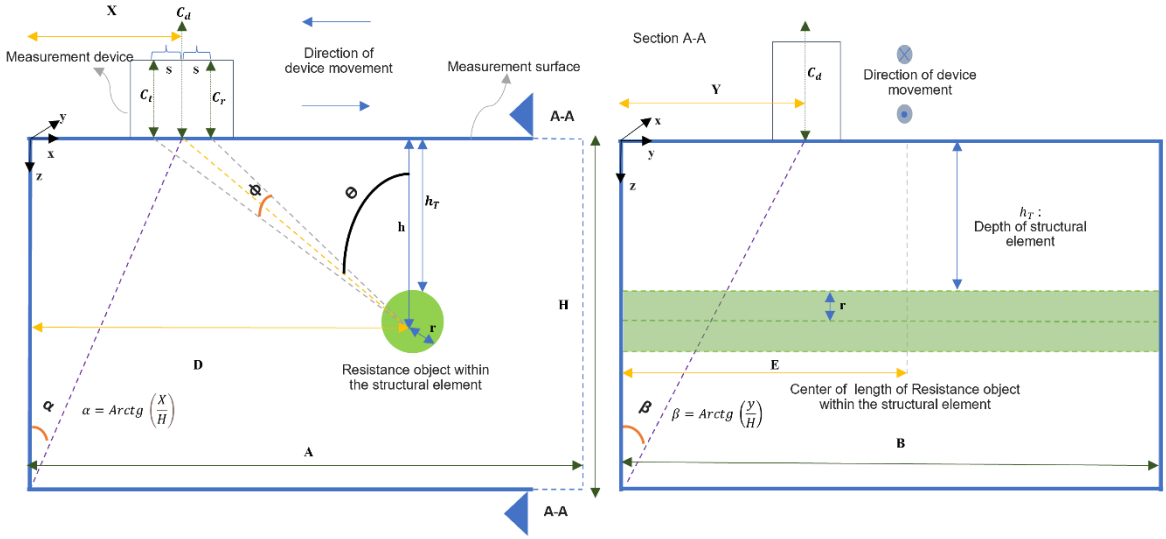

Fig. 4. General Schematic view of NDT Measurement Process.

The measurement result ($h_{measured}$) is calculated by eq. (5), which is related to the average of the time of flight of back wall (TOF_B) and the resistive object (TOF_Z), the changes in pulse shape (T_{chps}) and the lead time to determine time zero (T_{Offset}) of A-scan travel time in different position of measurement.

$$h_{measured} = \left(\frac{H}{C_{TOF_B}}\right) * C_{TOF_Z} \quad (5)$$

Where H is the specimen height and:

$$C_{TOF_B} = TOF_B - T_{Offset} - T_{chps} \quad (6)$$

$$C_{TOF_Z} = TOF_Z - T_{Offset} - T_{chps} \quad (7)$$

Due to the heterogeneous nature of concrete mixtures, a correction is applied to account for the assumption of constant velocity in wave propagation along the specimen. This correction can be expressed as:

$$CM_{h_T} = h_{measured} - \Delta_Z \quad (8)$$

Where Δ_Z is defined by the PMD description in the form of a function $\Delta_Z = f(\Theta, \varphi)$ and CM_{h_T} is the correct measurement result. This correction serves as an intercept for adjusting the measured depth.

2.2 Statistical Process

A series of experimental measurement on laboratory specimen is considered to investigate and extract the PMD description function for a modifier on the measurement results. Figure 5 illustrates the specifications of the experimental specimen, including its dimensions and the resistance object.

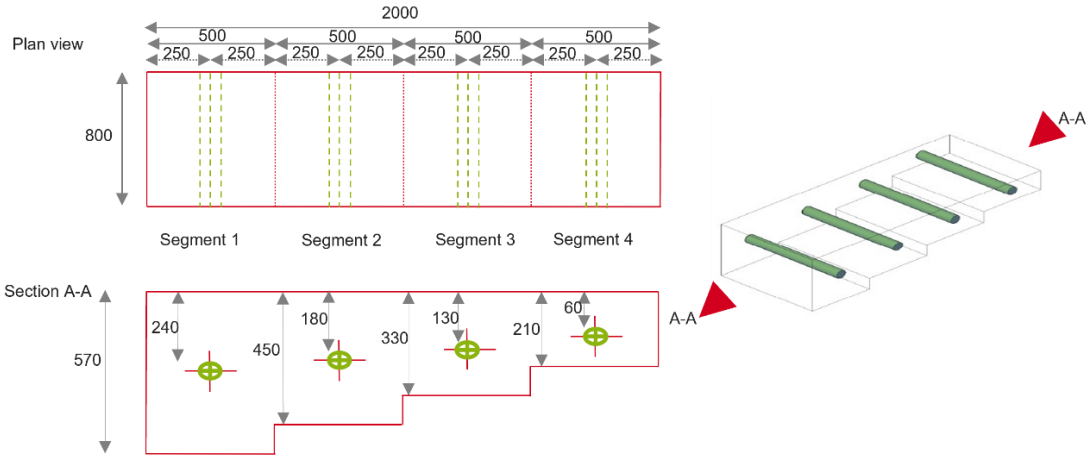

Fig. 5. The schematic view of laboratory specimen (dimensions in mm).

An Ultrasonic measurement process employing A1220 device system (with a sensor separation distance, $S = 3\ cm$) is conducted along four parallel lines ($y = 100,200,300$ and $400\ mm$) at each segment, with measurement intervals of $20\ mm$. PMD values for each measurement point are calculated based on the angles Θ and φ, along with the measured depth ($h_{measured}$).

$$\Theta = Arctg\left(\frac{|D-x|}{h_{measured}+r}\right) \quad (9)$$

$$\varphi = Arctg\left(\frac{h_{measured}+r}{D-x-S}\right) - Arctg\left(\frac{h_{measured}+r}{D-x+S}\right) \quad (10)$$

In the specimen, the accurate depth of tendon ducts (h_T) is known. However, the variance between the measured depth ($h_{measured}$) and h_T is calculated at each measurement point to derive the parameter Δ_Z. Figure 6 illustrates the scattering points of independent variations of PMD describing against Δ_Z, along with the best fit line in each data set cloud. The Linear Least Square Method (LLSM) provides a comprehensive understanding of the input dataset, covering all measurement points, and its ability to reveal the modifier function of Δ_Z. Additionally, it introduces the notion of lower and upper bands within a 95% confidence interval to mitigate uncertainties in the measurement process. This statistical approach entails analyzing the independent parameters of the PMD describer (Θ and φ) and their associated best-fit line interpreters ($\Theta^2$and φ^3) in a mathematical regression model against the dependent modifier function of Δ_Z.

$$\Delta_Z = 43.682 + 0.9008\,\Theta + 0.0114\,\Theta^2 - 5.0653\,\varphi + 0.0032\,\varphi^3 \quad (11)$$

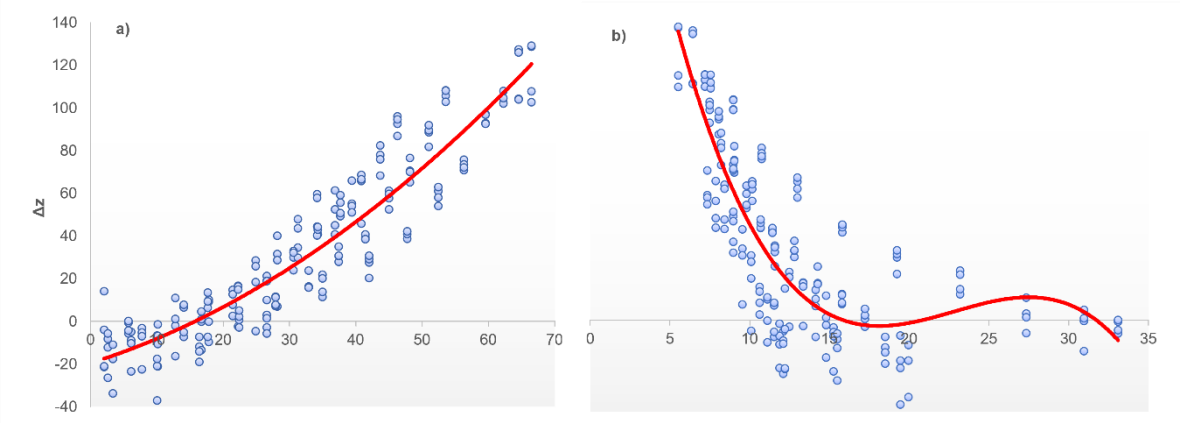

Fig. 6. Scattering diagram and best fit line for independent PMD variables against Δ_Z, a) Parameter of Θ(degree), b) Parameter of φ(degree).

Equation (11) represents the calculation of the modifier function by averaging the PMD describer values across all measurement points. The high values of R square (0.943) and adjusted R square (0.941) indicate that the function adeptly explains 94.3% of the observed variability in Δ_Z. The low significance F-value (6.181 E-115) of the regression equation emphasizes the strength of our model, indicating that the results are not merely coincidental. This instils confidence in engineers that our approach is robust for on-site inspections.

Table 1. Regression analysis summary output.

Variation	P-Value	Lower 95%	Upper 95%
Intercept	7.581E-17	34.305	53.059
Θ	3.964E-09	0.6132	1.1885
Θ^2	4.493E-07	0.0071	0.0157
φ	4.701E-32	-5.7603	-4.3703
φ^3	2.289E-24	0.0027	0.0037

Table 1 shows the regression equation's significance by demonstrating the meaningful relationship between independent and dependent variables, as evidenced by the low P-values. It also displays the lower and upper 95% confidence intervals to account for uncertainties in the measurement results.

3. Conclusion

In this study, we explore the maximum deflection at the mid-span of a main beam of a bridge. We utilize Euler beam theories (EBT) and take into account the impact of dynamic loading from traveling vehicles, by the moving masses theory. Our findings show the response of the bridge varies with the different placement of resistance elements within the bridge. We emphasize the significant influence of changes in the center of gravity of tendon ducts within the bridge structure. Our findings illustrate potential changes in bridge vibration response up to ±25%. It shows the critical role of understanding resistance element placement in the structural health monitoring (SHM) process. Such insights are crucial for extending the life cycle of bridge structures. To achieve these objectives, we investigate the suitability of Non-Destructive Testing (NDT) methods, which provide the benefit of inspecting structures without causing additional harm. However, the practical constraints and the work to reduce

measurement uncertainties demand substantial investments in both time and expertise. Our study addresses this challenge by examining the impact of measurement device positioning on data accuracy, introducing an adjustable term to enhance measurement precision. By applying statistical analysis and regression techniques, we establish robust mathematical relationships to modify measured depth in experimental measurements. Furthermore, we developed the step-by-step flowchart depicted in Figure 7, outlining a systematic approach to attain reliable measurement results. This framework not only simplifies the process but also facilitates the accurate determination of the positions of inner structural elements. This reduces the time needed by non-specialized personnel for NDT measurements. Such advancements are especially vital in structural on-site inspections, since prompt and accurate decisions, which are made without doing complex mathematical computations, are essential.

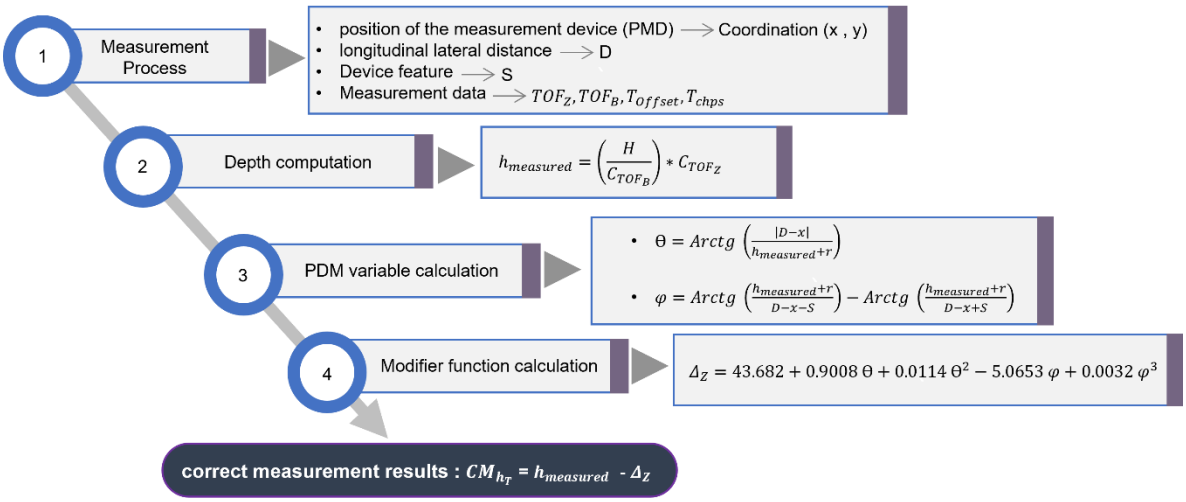

Fig. 7. Measurement process and calculation flowchart with PMD consideration.

References

[1] Nikkhoo A, Rofooei FR and Shadnam M (2007), "Dynamic behavior and modal control of beams under moving mass," J. Sound Vib., 306(3): 712-724.
[2] Pi Y, Ouyang H (2015), "Lyapunov-based boundary control of a multi-span beam subjected to moving masses," J. Vib. Control., 23(14): 2221-2234.
[3] Salcher P, Adam C (2015), "Modeling of dynamic train–bridge interaction in high-speed railways," Acta Mech 226(8): 2473–2495.
[4] Shrestha B (2015), "Seismic Response of Long Span Cable-stayed Bridge to Near-fault Vertical Ground Motions," KSCE J CIV ENG, 19(1): 180-187.
[5] Wang T, Li H, Ge Y (2015), "Vertical seismic response analysis of straight girder bridges considering effects of support structures," Earthquakes and Structures, 8(6): 1481-1497.
[6] Frýba L (1999), Vibration of solids and structures under moving loads, Thomas Telford, London.
[7] Vlada Gašić, Nenad Zrnić, Aleksandar Obradović, Srđan Bošnjak (2011), "Consideration of moving oscillator problem in dynamic responses of bridge cranes, " FME Transactions, 39:17-24.
[8] Nikkhoo A, Farazandeh A and Ebrahimzadeh Hassanabadi M (2014), "On the computation of moving mass/beam interaction utilizing a semi-analytical method," J. Braz. Soc. Mech. Sci. Eng., 38(3): 761-771.
[9] Ichikawa M, Miyakawa Y and Matsuda A (2000), "Vibration analysis of the continuous beam subjected to a moving mass," J. Sound Vib., 230(3): 493-506.
[10] Nikkhoo A, Eskandari A.B, Farazandeh A, Hajirasouliha I (2019), "Vibration control of bridges under simultaneous effects of earthquake and moving loads using steel pipe dampers" Journal of Vibration and Control, 25:2580-2594.
[11] Küttenbaum S, Braml T, Taffe A, Keßler S, Maack S. Reliability assessment of existing structures using results of nondestructive testing. Structural Concrete. 2021; 1–21.
[12] Küttenbaum, S.; Maack, S.; Braml, T.; Taffe, A.; Strübing, T. (2021), "Bewertung von Bestandsbauwerken mit gemessenen Daten, Teil 2". Berechnung der Tragwerkszuverlässigkeit unter Einbeziehung der ZfP-Messergebnisse. Beton- und Stahlbetonbau 116, H. 3, S. 183–199.

[13] Tianyu Xiang; Renda Zhao; and Tengfei Xu (2007), "Reliability Evaluation of Vehicle–Bridge Dynamic Interaction" Journal of structural Engineering, 133(8):1092-1099, DOI:10.1061/(ASCE)0733-9445(2007)133:8(1092)
[14] Stefan Küttenbaum, Stefan Maack, and Alexander Taffe (2022), "Approach to the development of a model to quantify the quality of tendon localization in concrete using ultrasound" MATEC Web of Conferences 364, 03007 ICCRRR 2022.